

# Elucidation of binding mode and three dimensional quantitative structure–activity relationship studies of a novel series of protein kinase B/Akt inhibitors

M. Muddassar · F. A. Pasha · M. M. Neaz · Y. Saleem · S. J. Cho

Received: 8 July 2008 / Accepted: 12 September 2008 / Published online: 29 November 2008  
© Springer-Verlag 2008

**Abstract** Protein kinase B (PKB; also known as Akt kinase) is located downstream in the PI-3 kinase pathway. Overexpression and constitutive activation of PKB/Akt leads to human prostate, breast and ovarian carcinomas. A series of 69 PKB/Akt inhibitors were examined to explore their binding modes using FlexX, and three-dimensional quantitative structure–activity relationship (3D-QSAR) studies based on comparative molecular field analysis (CoMFA) and comparative molecular similarity indices analysis (CoMSIA) were performed to provide structural insights into these compounds. CoMFA produced statistically significant results, with cross-validated  $q^2$  and non-cross validated correlation  $r^2$  coefficients of 0.53 and 0.95,

respectively. For CoMSIA, steric, hydrophobic and hydrogen bond acceptor fields jointly yielded ‘leave one out’  $q^2=0.51$  and  $r^2=0.84$ . The predictive power of CoMFA and CoMSIA was determined using a test set of 13 molecules, which gave correlation coefficients,  $r^2_{\text{predictive}}$  of 0.58 and 0.62, respectively. Molecular docking revealed that the binding modes of these molecules in the ATP binding sites of the Akt kinase domain were very similar to those of the co-crystallized ligand. The information obtained from 3D contour maps will allow the design of more potent and selective Akt kinase inhibitors.

**Keywords** 3D QSAR · Inhibitors · Molecular docking · Protein kinase B

M. Muddassar · F. A. Pasha · M. M. Neaz · Y. Saleem · S. J. Cho  
Future Fusion Technology Division,  
Computational Science Center,  
Korea Institute of Science and Technology,  
P.O. Box 131, Cheongryang,  
Seoul 130-650, South Korea

M. Muddassar  
e-mail: mmuddassar@kist.kr

M. Muddassar · M. M. Neaz · Y. Saleem  
School of Science, University of Science and Technology,  
Daejeon 305-333, South Korea

S. J. Cho (✉)  
College of Medicine, Chosun University,  
Gwangju 501-759, South Korea  
e-mail: chosj@chosun.ac.kr

S. J. Cho  
Research Center for Resistant Cells, Chosun University,  
Gwangju 501-759, South Korea

## Introduction

Protein kinase B (PKB; also known as Akt kinase) plays a pivotal role in the signal transduction pathways that are important for cellular transformation and tumor progression [1]. Akt1 is a serine/threonine protein kinase that was first discovered as the human homologue of the transforming gene in the AKT-v oncogenic virus isolated from a spontaneous thymoma in the AKR mouse [2]. Since the discovery of human Akt1, two additional mammalian Akt isoforms, designated Akt2 and Akt3, have been identified [3]. Phosphorylation at Ser and Thr is accompanied by the activation of Akt kinases [4]. Akt is located downstream of phosphoinositide 3-kinase (PI3K), therefore PI3K generates phosphorylated phosphatidylinositides in the cell membrane. The phosphorylated molecules binds to the amino terminal pleckstrin homology (PH) domain of Akt, which

activates phosphoinositide-dependent kinase (PKC). This activation leads to phosphorylation of the Thr residue of the membrane-bound Akt [5], whereas Ser is phosphorylated by integrin link kinase [6]. Mutation, deletion or overexpression of PKC isoforms is associated with the development of ovarian, prostate, and cervical tumours [7, 8].

RNA interference and Akt antibodies have been employed to study *akt* signaling pathways, cell survival, and tumor progression [9, 10]. In addition, chemically synthesized molecules have gained much attention for their ability to impede tumor progression when used as monotherapy or in combination with paclitaxel or rapamycin [11, 12]. To date, different PKC inhibitors have been developed that bind at different binding sites of the protein (i.e., ATP competitive or allosteric inhibitors) [12]. Since drug discovery focuses on the search for novel, more potent and selective inhibitors, quantitative structure activity relationships (QSAR) and three-dimensional QSAR (3D-QSAR) have become central approaches. QSAR techniques are largely used within framework of quantum QSAR [13], two dimensional-QSAR [14], hologram-QSAR, as well as 3D-QSAR [15]. In this paper, we investigated the binding modes of Akt inhibitors using molecular docking, and developed target-based 3D-QSAR models [16] to provide further structural insights.

## Materials and methods

### Data set and molecular modeling

A data set of 69 PKC inhibitors with their biological activities was obtained from the literature [17, 18]. The data set was randomly divided into a training set of 56 compounds to generate 3D QSAR models and a test set of 13 compounds to determine the predictive powers of these models. The  $IC_{50}$  (nM) values of the compounds were converted into the corresponding  $pIC_{50}$  values ( $pIC_{50} = -\log IC_{50}$ ) (Table 1). All molecular modeling studies and structures of these inhibitors were drawn with SYBYL 7.3 running on Linux cluster. These were initially minimized by Tripos force field [19], and Gasteiger-Hückel charges were assigned using the conjugate gradient method. The criterion of convergence was  $0.05 \text{ kcal mol}^{-1}$ .

### Molecular docking

For molecular docking studies, the coordinates of the recently reported receptor protein (PDB=2UZW) with the inhibitor was retrieved from the RCSB protein data bank ([www.rcsb.org](http://www.rcsb.org)). All water molecules were removed and the protein structure was repaired for missing residues without any modification to the C and N termini. Hydrogen atoms

were added to the protein atoms to satisfy their valences, and Gasteiger Hückel charges were assigned to the whole protein. Template-based molecular docking was performed with a radius of  $6.5 \text{ \AA}$ . All the molecules were docked using the FlexX program [20] without FlexX-pharm and spatial constraints in the protein. In docking simulations of each molecule, 100 conformations of every molecule were obtained by changing the default settings of the FlexX program. The best conformer of each molecule was identified and used for analysis.

### Molecular alignment for 3D-QSAR models

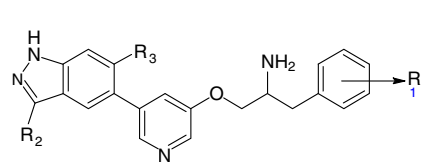
In the development of 3D-QSAR models, molecular alignment is a key step. Usually the molecules are aligned with a suitable conformational template that is thought to be the most bioactive, so that the inhibitors have comparable conformation and similar orientation in space [21]. In this study, the co-crystal structure was used as a template. The best conformer of each molecule was aligned using the common substructure based alignment method in SYBYL (Fig. 1).

### CoMFA and CoMSIA

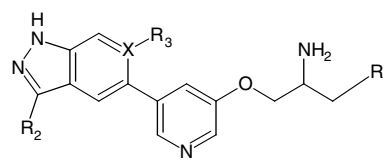
Lennard-Jones and Coulomb potentials based comparative molecular field analysis (CoMFA) were determined, and the steric as well as electrostatic energies were calculated using an  $sp^3$  carbon probe atom with a van der waals radius of  $1.52 \text{ \AA}$  and a +1 charge. The energies were truncated to  $\pm 30 \text{ kcal mol}^{-1}$  and the electrostatic contributions were ignored at lattice interactions with maximum steric interactions. The CoMFA were generated by a standard method within SYBYL. The comparative molecular similarity indices analysis (CoMSIA) models were also derived with the same lattice box used for CoMFA calculations. All five similarity indices (steric, electrostatic, hydrophobic, hydrogen bond donor, and hydrogen bond acceptor) were evaluated using the probe atom [22]. The CoMSIA models from hydrophobic and hydrogen bonds were calculated between the grid point and each atom of the molecule by a Gaussian function. The attenuation factor default value of 0.30 was used, which is the standard distance dependence of molecular similarity. The effect of using the standard attenuation factor is shown in contour maps with prominent molecular features.

### Partial least square analyses and validation of QSAR models

To derive 3D-QSAR models, CoMFA and CoMSIA descriptors were used as independent variables and  $pIC_{50}$  as the dependent variable. The partial least square (PLS)

**Table 1** Structures and biological activities of protein kinase B (PKB)/Akt inhibitors used for three-dimensional quantitative structure–activity relationship (3D-QSAR) analysis

A



B

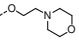
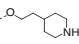
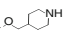
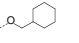
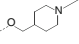
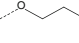
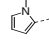
No.	Str.	R1	R2	R3	X	IC <sub>50</sub>
20*	A	4-Br-2-F	CH3	H	-	10
1	A	H	CH3	H	-	14
2*	A	3-F	CH3	H	-	8.4
3	A	2,3-di-F	CH3	H	-	8.5
4	A	2,4-di-F	CH3	H	-	21
5*	A	2,6-di-F	CH3	H	-	65.5
6	A	2,3,4-tri-F	CH3	H	-	12
7	A	2,4,6-tri-F	CH3	H	-	31
8	A	2-Cl	CH3	H	-	29
9	A	3-Cl	CH3	H	-	5.9
10*	A	4-Cl	CH3	H	-	11
11	A	2-Br	CH3	H	-	23
12	A	3-Br	CH3	H	-	2.1
13	A	4-Br	CH3	H	-	5
14	A	3-I	CH3	H	-	0.9
15*	A	3-Cl-4-F	CH3	H	-	3.1
16	A	4-Cl-3-F	CH3	H	-	3.6
17	A	2,3-(Cl)2	CH3	H	-	5.6
18	A	3,4-(Cl)2	CH3	H	-	1.8
19	A	3,5-(Cl)2	CH3	H	-	20.7
21	A	4-Br-3-F	CH3	H	-	1.3
22	A	2-Br-4,6-F2	CH3	H	-	49
23	A	5-F-2-Me	CH3	H	-	3.9
24	A	4-Br-3-Me	CH3	H	-	2.5
25*	A	4-F-3-Me	CH3	H	-	1
26	A	4-F-2-Me	CH3	H	-	6
27	A	3-F-4-Me	CH3	H	-	2.4
28*	A	2,4,6-(Me)3	CH3	H	-	39
29	A	5-F-2-OMe	CH3	H	-	7.7
30*	A	3-CF3	CH3	H	-	1.2
31	A	4-CF3	CH3	H	-	18
32	A	3,5-(CF3)2	CH3	H	-	57
33	A	3-CF3, 4-F	CH3	H	-	1.8
34	A	3-CF3, 5-F	CH3	H	-	13.3
35*	A	3-CF3, 6-F	CH3	H	-	1.2
36	A	4-CF3, 3-F	CH3	H	-	3.1
37	A	4-CF3, 2-F	CH3	H	-	12.1

method [23] was used to linearly correlate these descriptors to the inhibitory activity values. The CoMFA cutoff values were set to 30 kcal mol<sup>-1</sup> for both steric and electrostatic fields, and all fields were scaled by the default options in SYBYL. The cross validation analysis was performed using the leave-one-out (LOO) method [24], in which one compound is removed from the data set and its activity is predicted using the model derived from the rest of the dataset. The cross-validated correlation coefficient ( $q^2$ ) that resulted in optimum number of components and lowest

standard error of prediction were considered for further analysis and calculated using Eqs. 1 and 2:

$$q^2 = 1 - \frac{\sum (y_{pred} - y_{observed})^2}{\sum (y_{observed} - y_{mean})^2} \quad (1)$$

$$PRESS = \sum (y_{predicted} - y_{observed})^2 \quad (2)$$

No. Str.	R1	R2	R3	X	IC <sub>50</sub>	No. Str.	R1	R2	R3	X	IC <sub>50</sub>
38 A	2-OCF3	CH3	H	-	15.3	51 B	3-Indole	H	H	C	1.5
39 A	3-OCF3	CH3	H	-	3.3	52 B	3-Indole	Cl	H	C	1
40* A	4-OCF3	CH3	H	-	20.3	53 B	3-Indole	CF3	H	C	1.8
41 A	3-Ph	CH3	H	-	126	54 B	3-Indole	H	NO2	C	953
42 A	3,4-OCH2O-	CH3	H	-	42	55 B	3-Indole	H	NH2	C	51
43 A	2,3-OCF2O-	CH3	H	-	14	56 B	3-Indole	Cl	NH2	C	7.1
44 A	3,4-OCF2CF2O-	CH3	H	-	13	57 B	3-Indole	H	-	N	0.6
45* A		CH3	H	-	751	58 B	3-indole	CH3	-	N	0.34
46 A		CH3	H	-	290	59 B	Ph	H	-	N	223
47 A		CH3	H	-	6.8	60 B	Ph	CH3	-	N	25
48 A		CH3	H	-	1360	61 B	Ph	Cl	-	N	59
49 A		CH3	H	-	78	62 B	Ph	CH3	-	N	104
50 A		CH3	H	-	47	63 B	Ph	-H	-	N	223
						64* B	Ph	0	-	N	25
						65 B	Ph	-Cl	-	N	59
						66 B	Ph	vinyl	-	N	13
						67 B	Ph	2-Furyl-	-	N	6.1
						68 B	Ph		-	N	228
						69* B	Ph	-Ph	-	N	8.3

\* Test set Compounds

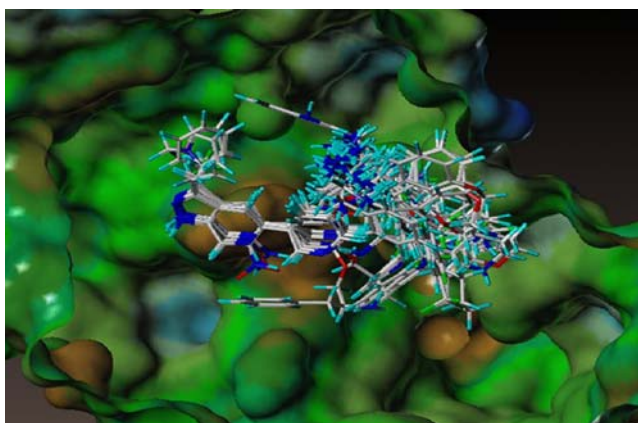


**Fig. 1** Alignment of molecules within the active site of the protein for three-dimensional quantitative structure–activity relationship (3D-QSAR) analyses

Where  $y_{\text{pred}}$ ,  $y_{\text{actual}}$ , and  $y_{\text{mean}}$  are the predicted, actual, and mean values of the target property ( $\text{pIC}_{50}$ ), respectively, and PRESS is the sum of squares residuals of actual and predicted activities of test set compounds. The non-cross-validated PLS analyses were performed with a column filter value of 2.0 to reduce analysis time with little effect on the  $q^2$  values. To further assess the robustness and statistical confidence of the derived models, bootstrapping analysis for 100 runs was performed. To assess the predictive power of the 3D-QSAR models derived using the training set, biological activities of an external test set of 13 molecules were predicted. The predictive ability of the models was expressed by the predictive  $r^2$  value, which is analogous to cross-validated  $r^2$  ( $q^2$ ), using Eq. 3:

$$r_{\text{pred}}^2 = \frac{SD - \text{PRESS}}{SD} \quad (3)$$

Where SD is the sum of the squared deviations between the biological activities of the test set and mean activities of the training molecules, and PRESS is the sum of squared deviation between predicted and actual activities of the test set molecules.

## Results and discussion

### Elucidation of binding mode

The overall fold and structure of PKB is very similar to that of PKA [25, 26] although there are some differences at the N-terminus of PKA, which contains an additional 18  $\alpha$ -helical amino acid residues. These two homologous kinase structures possess nearly identical ATP-binding sites, with a difference of just three residues within the active site (substitutions of Val123 by Ala232, Val104 by Thr213, and Leu173 by Met282 in PKB [25]). Another study reported that residues Glu-121 and Val-123 at the hinge region of Akt are crucial to activity and establish important hydrogen bonds with pyridine-pyrazolopyridine-based inhibitors [27]. PKB/Akt inhibitors typically bind to the two binding sites, namely the ATP binding site and the allosteric pocket, to block activity. We first docked 2UZW, the co-crystal ligand and most active ligand in the protein, to validate the efficiency of the FlexX docking program for these inhibitors. The conformational comparison of these two ligands having similar binding modes at the ATP binding site is depicted in Fig. 2. In molecular docking simulation studies, 100 conformers for each inhibitor were generated. The primary criterion for the selection of the best conformer was the visual resemblance to the co-crystallized ligand as

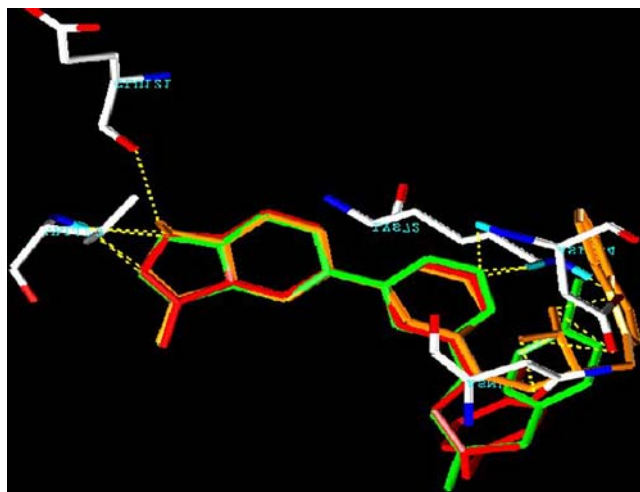


**Fig. 2** Conformational comparison of co-crystal (orange), docked co-crystal (green) and docked most active compound-58 (red) using fFlexX

**Table 2** Statistical summary of comparative molecular field analysis (CoMFA)-based models.  $q^2$  Cross validated correlation coefficient after leave-one-out (LOO) procedure,  $n$  optimal number of components,  $r^2$  correlation coefficient,  $SEE$  standard error of estimate,  $F$  Fischer's  $F$  value for test of significance,  $r_{bs}^2$  coefficient of determination after 100 bootstrapping runs,  $r_{pred}^2$  predicted correlation coefficient for test set of compounds,  $GS$  grid size

	GS=2.0 Å	GS=0.5 Å	GS=1 Å	GS=1.5 Å
$q^2$	0.53	0.49	0.49	0.47
$n$	8	10	8	6
$r^2$	0.95	0.97	0.94	0.90
$SEE$	0.18	0.13	0.19	0.24
$F$ -value	98	159.43	90.88	71.53
$r_{bs}^2$	0.96	0.98	0.96	
$r_{pred}^2$	0.58	0.59	0.56	0.40
Contributions				
Steric	0.47	0.55	0.49	0.56
Electrostatic	0.53	0.45	0.51	0.44

well as the distance to key residues of the active site, while the total score was used as a secondary criterion. Previous molecular docking studies of these inhibitors demonstrated that all the compounds have similar binding mode and hydrogen bonding behavior [19].

### 3D-QSAR model

Initially, the CoMFA and CoMSIA models were developed using the 56 molecules of the training set. Models based on these compounds yielded low  $q^2$  values of 0.29 and 0.31, respectively. Therefore, to generate reasonable models, compounds with a residual value between experimental and predicted pIC50 >1 logarithmic unit in the CoMFA or

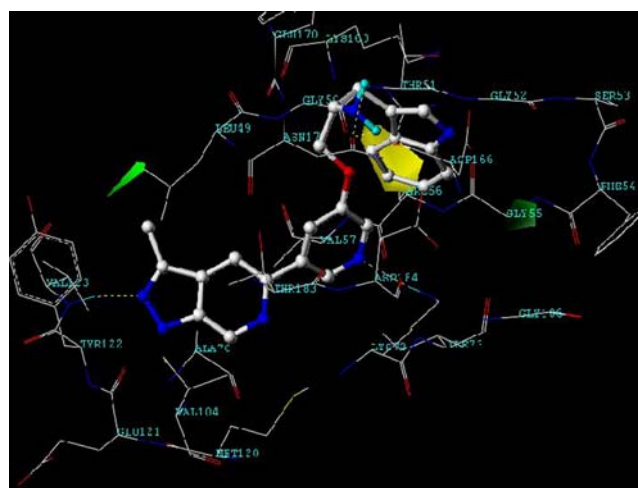


**Fig. 3** Comparative molecular field analysis (CoMFA) steric contour maps around the most active molecule superimposed on the active site of the protein

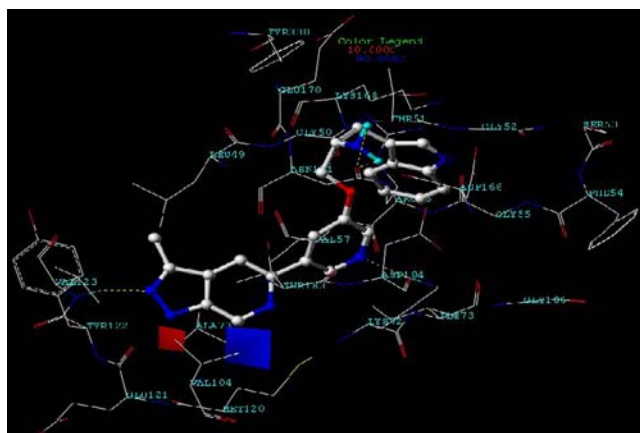


**Fig. 4** CoMFA electrostatic contour maps around the most active molecule superimposed on the active site of the protein

CoMSIA model were considered outliers. Accordingly, compounds **47**, **48**, **55**, and **68** were considered to be outliers [28]. Outliers may arise as a consequence of incorrectly measured inhibitory concentrations, different binding conformations, or significant differences in physicochemical properties [29]. Discarding the outliers and re-derivation of the 3D-QSAR model using the remaining compounds

yielded much higher cross-validated  $q^2$  values of 0.53 and 0.51 for the CoMFA and CoMSIA models, respectively. Thus, subsequent analyses were based on the 52 non-outlier compounds, and these models were also used to predict the activity of test set of compounds.

### CoMFA

In CoMFA models, the steric and electrostatic fields are correlated individually and in combination with biological activities. The grid size was varied to obtain more pronounced models. When the 0.5 Å grid size was used initially, the steric and electrostatic fields jointly gave  $q^2=0.49$  and  $r^2=0.97$  with  $n=10$ . To improve the result and reveal relationships more prominently, grid sizes of 1.0 Å, 1.5 Å, and 2.0 Å were used. A grid size of 2.0 Å produced significant results ( $q^2=0.53$ ,  $r^2=0.95$ ,  $r_{bs}^2=0.96$ ) (Table 2), because larger molecules warrant larger spacing, while for smaller molecules (<20 heavy atoms) a finer grid spacing (e.g., 1.5 Å) may be appropriate [30], and the charge transfer and electrostatic interaction may be local or fragment-based. In the former case, the small grid size yields good statistics, as there will be a sharp interaction due to a single atom. If more than one atom is involved in

**Table 3** Statistical summary of comparative molecular similarity indices analysis (CoMSIA)-based models.  $q^2$  Cross-validated correlation coefficient after LOO procedure,  $r^2$  correlation coefficient,  $n$  optimal number of components,  $SEE$  standard error of estimate,  $F$

Fischer's  $F$  value for test of significance,  $r_{pred}^2$  predicted correlation coefficient for test set of compounds. Field contributions:  $S$  steric field,  $E$  electrostatic field,  $H$  hydrophobic field,  $D$  H-bond donor field,  $A$  H-bond acceptor field

Fields	$q^2$	$n$	$r^2$	$SEE$	F-value	$r_{pred}^2$	S	E	H	D	A
S	0.24	4	0.56	0.51	14.85	–	1	–	–	–	–
E	–0.23	2	0.47	0.55	22.30	–	–	1	–	–	–
H	0.44	4	0.75	0.39	34.68	0.55	–	–	1	–	–
D	–0.02	5	0.56	0.52	11.56	–	–	–	–	1	–
SE	0.25	10	0.94	0.20	64.07	–	0.50	0.50	–	–	–
SD	0.41	10	0.84	0.32	22.40	0.35	0.37	–	–	0.63	–
SA	0.42	8	0.80	0.36	21.65	0.40	0.35	–	–	–	0.65
SH	0.49	5	0.80	0.35	36.50	0.40	0.30	–	0.70	–	–
EH	0.25	3	0.70	0.41	37.35	–	–	0.39	0.61	–	–
EDA	0.09	2	0.35	0.66	13.38	–	–	0.20	–	0.41	0.39
EHD	0.18	3	0.72	0.40	41.70	–	–	0.20	0.51	0.29	–
EHA	0.28	3	0.67	0.44	33.03	–	–	0.30	0.45	–	0.25
SHE	0.40	10	0.96	0.16	106	0.41	0.23	0.41	0.36	–	–
SED	0.34	8	0.92	0.22	64	–	0.21	0.28	–	0.34	–
SEA	0.18	2	0.46	0.55	21	–	0.21	0.28	–	–	0.51
SHD	0.43	5	0.84	0.31	47	0.67	0.17	–	0.48	0.35	–
SHA	0.51	6	0.84	0.31	40	0.62	0.22	–	0.50	–	0.28
SDA	0.37	10	0.83	0.34	19.86	–	0.39	–	–	0.45	0.26
SEHD	0.30	6	0.91	0.24	73	–	0.16	0.25	0.30	0.19	–
SEHA	0.42	10	0.96	0.15	114.64	0.45	0.18	0.33	0.30	–	0.19
SHDA	0.40	6	0.86	0.30	45.10	0.67	0.16	–	0.38	0.31	0.15
SEDA	0.30	10	0.93	0.22	53	–	0.23	0.35	–	0.25	0.16
EHDA	0.21	2	0.51	0.53	25.34	–	–	0.14	0.33	0.28	0.25
SEHDA	0.31	10	0.96	0.16	101.7	–	0.16	0.24	0.25	0.22	0.13

such an interaction and a zone of ligand participation in electrostatic interaction exists, then a large grid size would be more meaningful. Thus, the selection of grid spacing is an end-user decision. Furthermore, the predictive power ( $r^2_{\text{predictive}} = 0.58$ ) of this model was determined by the test set of 13 compounds. The comparison of predicted and experimental activities is presented in Tables 4 and 5.

#### CoMFA contour maps

CoMFA contour maps were generated to visualize the best fitted 3D-QSAR model for steric and electrostatic fields effects on the 58 most active molecules of the series (Figs. 3, 4). The CoMFA green contours indicate the steric bulk area favoring better activity while the yellow contours denote the smaller groups. In Fig. 3, the green contour that appeared around the methyl group of the pyrazolo-pyridine ring indicates that a bulky group around this position might beneficially affect activity. As this polyhedron is directed towards a small residue (Leu-49), sufficient space is provided to accommodate the bulky group at this position. Similarly, a green contour was evident near the indole ring and was directed towards Gly-55, which was indicative of a demand for steric bulk to improve the activity of further compounds. A yellow contour near positions 5 and 6 of the indole ring illustrated that the steric bulk group was not favorable for higher activity at these sites. Figure 4 illustrates the CoMFA electrostatic map with a highly active compound within the active site. In this figure, the blue contour depicts areas that are favorable for positive groups and the red contour denotes the area favorable for negative groups. A red contour appeared near to the nitrogen moiety of the pyrazolo pyridine ring, directed towards Ala-70, which is evidence that a positive group may facilitate binding with the protein.

#### CoMSIA

In a similar manner, CoMSIA was also performed, and the five fields (steric, electrostatic, hydrophobic, hydrogen bond donor, and acceptor) descriptors were related with the variation of activities using PLS analyses. Since CoMFA gave the best result with a grid size of 2.0 Å, the same box size was used in CoMSIA, and the different fields were related individually and in different combinations. Table 3 summarizes the regression analyses. Individual fields displayed low  $q^2$  values as compared to combined fields, and the best fitted model was obtained with steric, hydrophobic, and hydrogen bond acceptor field effects ( $q^2=0.51$ ,  $n=6$ ,  $r^2=0.84$  and  $r^2_{\text{predictive}} = 0.62$ ). The steric, hydrophobic and hydrogen bond acceptor field effect based model was used to predict the activities of training and test sets reported in Tables 4 and 5.

**Table 4** Observed and predicted biological activities with their residuals by CoMFA and CoMSIA models of training set compounds. PA Predicted activity

Compound	pIC <sub>50</sub>	PA <sub>CoMFA</sub>	Residual	PA <sub>CoMSIA</sub>	Residual
1	-1.15	-0.85	-0.30	-1.15	0.00
3	-0.93	-1.07	0.14	-1.10	0.17
4	-1.32	-1.24	-0.08	-1.36	0.04
6	-1.08	-0.90	-0.18	-0.96	-0.12
7	-1.50	-1.70	0.20	-1.59	0.09
8	-1.46	-1.27	-0.19	-1.52	0.06
9	-0.77	-0.47	-0.30	-0.58	-0.19
11	-1.36	-1.14	-0.22	-1.61	0.25
12	-0.32	-0.47	0.15	-0.43	0.11
13	-0.70	-0.65	-0.05	-0.67	-0.03
14	0.04	-0.27	0.31	-0.07	0.11
16	-0.56	-0.40	-0.16	-0.43	-0.13
17	-0.75	-0.82	0.07	-0.84	0.09
18	-0.25	-0.27	0.02	-0.23	-0.02
19	-1.32	-1.33	0.01	-1.16	-0.16
21	-0.11	-0.36	0.25	-0.31	0.20
22	-1.69	-1.56	-0.13	-1.46	-0.24
23	-0.59	-0.87	0.28	-0.79	0.20
24	-0.40	-0.62	0.22	-0.56	0.16
26	-0.78	-0.71	-0.07	-0.61	-0.17
27	-0.38	-0.46	0.08	-0.27	-0.11
29	-0.89	-1.16	0.27	-1.13	0.24
31	-1.25	-0.72	-0.53	-0.93	-0.32
32	-1.76	-1.79	0.03	-1.49	-0.27
33	-0.25	-0.26	0.01	-0.43	0.18
34	-1.12	-1.01	-0.11	-1.03	-0.10
36	-0.49	-0.49	0	-0.51	0.02
37	-1.08	-1.26	0.18	-1.34	0.26
38	-1.18	-1.26	0.08	-1.00	-0.18
39	-0.52	-0.50	-0.02	-0.53	0.01
41	-2.10	-1.96	-0.14	-2.14	0.04
42	-1.62	-1.52	-0.1	-1.56	-0.06
43	-1.15	-1.21	0.06	-1.28	0.13
44	-1.14	-1.21	0.07	-1.04	-0.10
46	-2.46	-2.36	-0.10	-2.37	-0.09
47 <sup>a</sup>	-0.83	-1.80	0.97	-1.86	1.03
48 <sup>a</sup>	-3.13	-1.86	-1.27	-1.84	-1.29
49	-1.89	-1.87	-0.02	-1.87	-0.02
50	-1.67	-1.81	0.14	-1.66	-0.01
51	-0.18	-0.31	0.13	-0.34	0.16
52	0	-0.05	0.05	-0.14	0.14
53	-0.25	-0.16	-0.09	-0.21	-0.04
54	-2.98	-3.01	0.03	-3.04	0.06
55 <sup>a</sup>	-1.71	-0.90	-0.81	-0.68	-1.03
56	-0.85	-0.60	-0.25	-0.49	-0.36
57	0.22	0.36	-0.14	-0.12	0.34
58	0.47	0.26	0.21	0.67	-0.20
59	-2.35	-2.27	-0.08	-2.11	-0.25
60	-1.40	-1.35	-0.05	-1.33	-0.07
61	-1.77	-1.99	0.22	-1.93	0.16
62	-2.01	-2.00	-0.01	-1.94	-0.07
63	-2.35	-2.31	-0.04	-2.25	-0.10
65	-1.77	-1.89	0.12	-2.08	0.31
66	-1.11	-0.98	-0.13	-1.07	-0.04
67	-0.78	-0.75	-0.03	-0.68	-0.10
68 <sup>a</sup>	-2.36	-0.73	-1.63	-0.49	-1.87

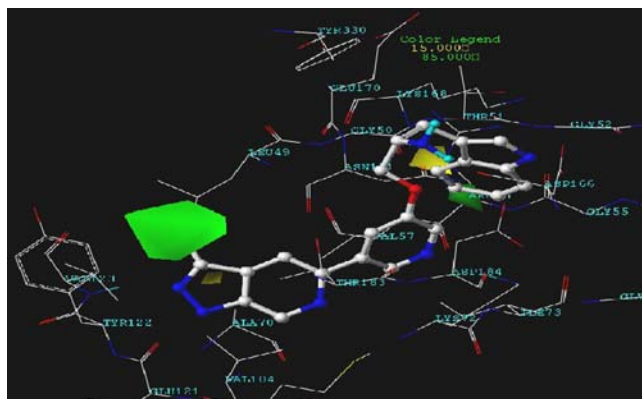
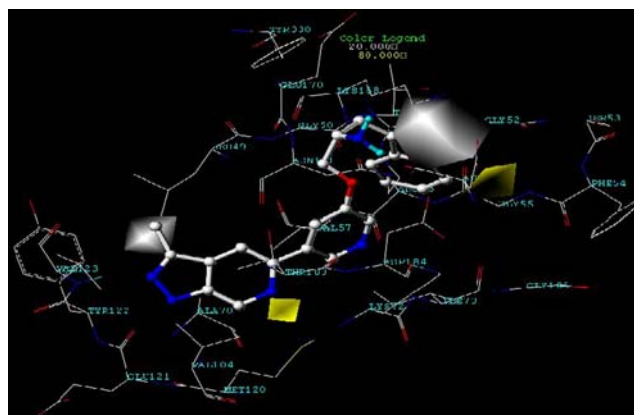
<sup>a</sup>Outliers

**Table 5** Observed and predicted biological activities with their residuals by CoMFA and CoMSIA models of test set compounds

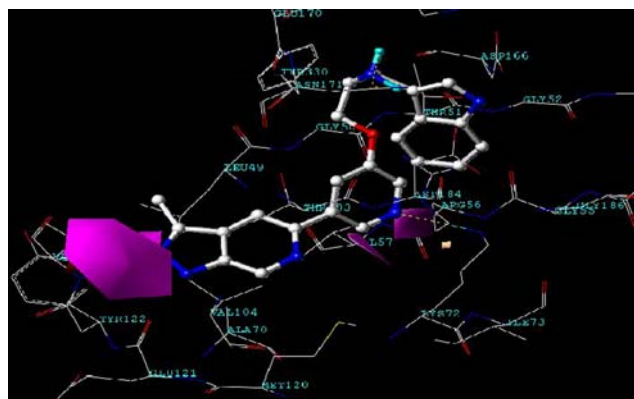
Compound	pIC50	PA <sub>CoMFA</sub>	Residual	PA <sub>CoMSIA</sub>	Residual
2	-0.92	-0.56	-0.36	-0.77	-0.15
5	-1.82	-1.56	-0.26	-1.67	-0.15
10	-1.04	-0.78	-0.26	-0.81	-0.23
15	-0.49	-0.29	-0.20	-0.43	-0.07
20	-1.00	-1.23	0.23	-1.05	0.05
25	-1.04	-0.75	-0.29	-0.91	-0.13
28	-1.51	-0.64	-0.87	-0.08	-1.43
30	-0.08	-0.60	0.52	-0.53	0.45
35	-0.08	-0.64	0.56	-0.76	0.68
40	-1.31	-1.55	0.24	-1.01	-0.30
45	-2.88	-2.12	-0.76	-2.40	-0.48
64	-1.40	-1.60	0.20	-1.38	-0.02
69	-0.92	-0.60	-0.32	-0.39	-0.53

### CoMSIA contour maps

CoMSIA contour maps developed with the best model are displayed in Figs. 5, 6 and 7. In general, the steric and electrostatic field distributions of CoMSIA and CoMFA maps were positioned at the same place in space. In Figs. 3, 4 and 5, contour maps appear approximately at the same place, providing a strong indication for further modification of these compounds to improve their activity. In the CoMSIA model, green contours favored the steric bulk group and yellow favored the small group. In the hydrophobic map depicted in Fig. 6, the white contour represents hydrophobic groups and the yellow contour indicates areas favorable for hydrophilic groups. The green and white contour maps were coincident in the vicinity of C-1 of the pyrazolo-pyridine ring in Figs. 5 and 6, which indicated a favorable region for steric bulk groups; a white contour appearing at same sites indicated that a hydrophobic group might be helpful for higher activity of the newly synthesized compounds. Similarly, the nitrogen moiety of

**Fig. 5** CoMSIA steric contour maps around the most active molecule, superimposed on the active site of the protein**Fig. 6** CoMSIA hydrophobic contour maps around the most active molecule, superimposed on the active site of the protein

pyridine of the pyrazolo-pyridine ring and carbon-6 of the indole ring yielded a yellow contour, indicating that a hydrophilic group would enhance activity. The role of hydrophobic and steric field effects can be explained by analyzing molecules 54, 55, and 56 in Table 1. Molecule 56 has hydrophobic groups in the space of white contour and hydrophilic groups at the yellow contour of the ring, making it the most active among the three compounds. Similarly, the bulky group (-Cl) at C-1 of pyrazolo-pyridine of molecule 54 rendered it the more active than other two molecules of the same scaffold. Figure 7 displays the hydrogen bond acceptor map; a magenta contour indicates areas favorable for hydrogen bond acceptor groups, while the orange contour depicts the areas favorable for hydrogen bond donor groups. A magenta contour near to pyrazolo-pyridine ring was directed towards the hinge region (Met-120 to Val-124); a hydrogen bond acceptor group would increase binding in this region. Similarly, the hydrogen bond accepting group at the nitrogen moiety of the pyridine ring might increase biological activity, and would exhibit strong hydrogen bonding with Lys-72. These findings agree with the docking studies shown in Fig. 1.

**Fig. 7** CoMSIA hydrogen bond acceptor contour maps around the most active molecule superimposed on the active site of the protein



## Conclusion

Molecular docking was performed without applying any constraint to the protein for all compounds. Our docking results prove that all molecules possess the same binding mode and have same hydrogen bonding contacts within the PKB protein as reported in the literature. The molecular fields were calculated using CoMFA and CoMSIA, and these values were correlated with biological activity. The CoMFA and CoMSIA models exhibited good statistical results. The contour maps of CoMFA and CoMSIA models demonstrated that electrostatic, steric, and hydrophobic interactions are dominant for the binding of inhibitors with the enzyme. The present study provides valuable information about the enhancement of activity and selectivity of these inhibitors. For example, substitution of hydrophobic and steric bulk groups at the pyrazolo-pyridine ring and substitution of hydrophilic groups at the nitrogen moiety of the pyrazolo-pyridine ring pyridine residue will enhance the biological activity of these compounds. Similarly, hydrogen bond acceptor groups located at the hinge contact region of the molecules will increase the activity of the newly synthesized compounds.

**Acknowledgments** This work was supported by a Korea Science and Engineering Foundation(KOSEF) grant funded by the Korean government (MEST) through the Research Center for Resistant Cells (R13-2003-009). We are thankful to Hwan Won Jung and Jung Soo Oh for assistance in using the computational facilities.

## References

- Hemmings BA (1997) Akt signaling: linking membrane events to life and death decisions. *Science* 275:628–630. doi:10.1126/science.275.5300.628
- Burgering BM, Coffey PJ (1995) Protein kinase B (c-Akt) in phosphatidylinositol-3-OH kinase signal transduction. *Nature* 376:599–602. doi:10.1038/376599a0
- Nakatani K, Sakaue H, Thompson DA, Weigel RJ, Roth RA (1999) Identification of a human Akt3 (protein kinase B gamma) which contains the regulatory serine phosphorylation site. *Biochem Biophys Res Commun* 257:906–910. doi:10.1006/bbrc.1999.0559
- Alessi DR, Andjelkovic M, Caudwell B, Cron P, Morrice N, Cohen P et al (1996) Mechanism of activation of protein kinase B by insulin and IGF-1. *EMBO J* 15:6541–6551
- Galetic I, Andjelkovic M, Meier R, Brodbeck D, Park J, Hemmings BA (1999) Mechanism of protein kinase B activation by insulin/insulin-like growth factor-1 revealed by specific inhibitors of phosphoinositide 3-kinase-significance for diabetes and cancer. *Pharmacol Ther* 82:409–425. doi:10.1016/S0163-7258(98)00071-0
- Yoganathan TN, Costello P, Chen X, Jabali M, Yan J, Leung D et al (2000) Integrin-linked kinase (ILK): a “hot” therapeutic target. *Biochem Pharmacol* 60:1115–1119. doi:10.1016/S0006-2952(00)00444-5
- Samuels Y, Wang Z, Bardelli A, Silliman N, Ptak J, Szabo S et al (2004) High frequency of mutations of the PIK3CA gene in human cancers. *Science* 304:554. doi:10.1126/science.1096502
- Workman P, Clarke PA, Guillard S, Raynaud FI (2006) Drugging the PI3 kinase. *Nat Biotechnol* 24:794–796. doi:10.1038/nbt0706-794
- Hisamoto K, Ohmichi M, Kurachi H, Hayakawa J, Kanda Y, Nishio Y et al (2001) Estrogen induces the Akt-dependent activation of endothelial nitric-oxide synthase in vascular endothelial cells. *J Biol Chem* 276:3459–3467. doi:10.1074/jbc.M005036200
- Jeong SJ, Dasgupta A, Jung KJ, Um JH, Burke A, Park HU et al (2008) PI3K/AKT inhibition induces caspase-dependent apoptosis in HTLV-1-transformed cells. *Virology* 370:264–272. doi:10.1016/j.virol.2007.09.003
- Zhao Z, Leister WH, Robinson RG, Barnett SF, Defeo-Jones D, Jones RE et al (2005) Discovery of 2,3,5-trisubstituted pyridine derivatives as potent Akt1 and Akt2 dual inhibitors. *Bioorg Med Chem Lett* 15:905–909. doi:10.1016/j.bmcl.2004.12.062
- Lindsley CW, Zhao Z, Leister WH, Robinson RG, Barnett SF, Defeo-Jones D et al (2005) Allosteric Akt (PKB) inhibitors: discovery and SAR of isozyme selective inhibitors. *Bioorg Med Chem Lett* 15:761–764. doi:10.1016/j.bmcl.2004.11.011
- Pasha FA, Muddassar M, Cho SJ, Ahmad K, Beg Y (2008) 3D and quantum QSAR of non-benzodiazepine compounds. *Eur J Med Chem* (2008) 43:2361–2372
- Pasha FA, Neaz MM, Cho SJ, Kang SB (2007) Quantitative structure activity relationship (QSAR) study of estrogen derivatives based on descriptors of energy and softness. *Chem Biol Drug Des* 70:520–529. doi:10.1111/j.1747-0285.2007.00593.x
- Marshall GR, Cramer RD 3rd (1988) Three-dimensional structure-activity relationships. *Trends Pharmacol Sci* 9:285–289. doi:10.1016/0165-6147(88)90012-0
- Muddassar M, Pasha FA, Chung HW, Yoo KH, Oh CH, Cho SJ (2008) Receptor guided 3D-QSAR: a useful approach for designing of IGF-1R inhibitors. *J Biomed Biotechnol* 2008:837653. doi:10.1155/2008/837653
- Zhu GD, Gong J, Gandhi VB, Woods K, Luo Y, Liu X et al (2007) Design and synthesis of pyridine-pyrazolopyridine-based inhibitors of protein kinase B/Akt. *Bioorg Med Chem* 15:2441–2452. doi:10.1016/j.bmc.2007.01.010
- Zhu GD, Gandhi VB, Gong J, Thomas S, Woods KW, Song X et al (2007) Syntheses of potent, selective, and orally bioavailable indazole-pyridine series of protein kinase b/akt inhibitors with reduced hypotension. *J Med Chem* 50:2990–3003. doi:10.1021/jm0701019
- Clark M, Cramer RD, Vanopdenbosch N (1989) Validation of the general-purpose tripos 5.2 force-field. *J Comput Chem* 10:982–1012. doi:10.1002/jcc.540100804
- Rarey M, Kramer B, Lengauer T, Klebe G (1996) A fast flexible docking method using an incremental construction algorithm. *J Mol Biol* 261:470–489. doi:10.1006/jmbi.1996.0477
- Zou XJ, Lai LH, Jin GY, Zhang ZX (2002) Synthesis, fungicidal activity, and 3D-QSAR of pyridazinone-substituted 1,3,4-oxadiazoles and 1,3,4-thiadiazoles. *J Agric Food Chem* 50:3757–3760. doi:10.1021/jf0201677
- Klebe G, Abraham U, Mietzner T (1994) Molecular similarity indexes in a comparative-analysis (Comsia) of drug molecules to correlate and predict their biological-activity. *J Med Chem* 37:4130–4146. doi:10.1021/jm00050a010
- Geladi P, Xie YL, Polissar A, Hopke P (1998) Regression on parameters from three-way decomposition. *J Chemometr* 12:337–354. doi:10.1002/(SICI)1099-128X(199809/10)12:5<337::AID-CEM517>3.0.CO;2-1
- Cramer RD, Bunce JD, Patterson DE, Frank IE (1988) Cross-validation, bootstrapping, and partial least-squares compared with multiple-regression in conventional qsar studies. *Quant Struct Activity Relationships* 7:18–25. doi:10.1002/qsar.19880070105

25. Gassel M, Breitenlechner CB, Ruger P, Jucknischke U, Schneider T, Huber R et al (2003) Mutants of protein kinase A that mimic the ATP-binding site of protein kinase B (AKT). *J Mol Biol* 329:1021–1034. doi:10.1016/S0022-2836(03)00518-7
26. Yang J, Cron P, Thompson V, Good VM, Hess D, Hemmings BA et al (2002) Molecular mechanism for the regulation of protein kinase B/Akt by hydrophobic motif phosphorylation. *Mol Cell* 9:1227–1240. doi:10.1016/S1097-2765(02)00550-6
27. Davies TG, Verdonk ML, Graham B, Saalau-Bethell S, Hamlett CC, McHardy T et al (2007) A structural comparison of inhibitor binding to PKB, PKA and PKA-PKB chimera. *J Mol Biol* 367:882–894. doi:10.1016/j.jmb.2007.01.004
28. Bang SJ, Cho SJ (2004) Comparative molecular field analysis (CoMFA) and comparative molecular similarity index analysis (CoMSIA) study of mutagen X. *Bull Korean Chem Soc* 25:1525–1530
29. Liao CZ, Xie AH, Zhou JJ, Shi LM, Li ZB, Lu XP 3rd (2004) QSAR studies on peroxisome proliferator-activated receptor gamma agonists using CoMFA and CoMSIA. *J Mol Model* 10:165–177. doi:10.1007/s00894-003-0175-4
30. Ekins S, Waller CL, Swaan PW, Cruciani G, Wrighton SA, Wikel JH (2000) Progress in predicting human ADME parameters in silico. *J Pharmacol Toxicol Methods* 44:251–272. doi:10.1016/S1056-8719(00)00109-X